Ecological Indicators 113 (2020) 106215

Contents lists available at ScienceDirect

Ecological Indicators

journal homepage: www.elsevier.com/locate/ecolind

Vegetation growth variation in relation to topography in Horqin Sandy Land

Jiaqi Fan[a], Yan Xu[a,b,*], Haoyuan Ge[a], Wei Yang[a]

[a] College of Land Science and Technology, China Agricultural University, Beijing 100193, China
[b] Key Laboratory of Agricultural Land Quality and Monitoring of Nature Resource, Beijing 100193, China

ARTICLE INFO

Keywords:
GRNDVI
Vegetation growth
Wetness
Topography index
Horqin Sandy Land

ABSTRACT

Water availability is a major limiting factor for vegetation growth in semi-arid areas. Soil moisture availability is related to topography, which therefore, influences vegetation growth. To examine the response of vegetation growth to topography, we calculated an index of vegetation growth (GRNDVI) and analyzed its distribution along a topography index in Horqin Sandy Land, Inner Mongolia, China. Cropland growth improved and then deteriorated as topography increased, while wetness initially increased and then declined. In contrast, grassland growth initially declined and then improved with increasing topography, while wetness continuously declined. Grassland growth was affected by soil moisture and by different plant species. Cover and height of herbaceous species decreased from flat to hilltop while the cover and height of shrub species increased, especially those species with stronger drought tolerance. Different optimal land use scenarios were proposed based on water availability and topographic position. In the lowest areas, wetlands are proposed to promote natural habitat for aquatic plants and animals. In low areas, water facilities could be constructed and crops planted to supply food. In the middle area, grassland should be utilized to provide some pastures. In the upper and highest areas, drought tolerant shrubs should be planted to stabilize slopes and enhance native biodiversity and ecological integrity. The study could be used as a functional model to reduce desertification in semi-arid areas through optimizing land utilization, maintaining and enhancing ecological integrity and promoting sustainable development.

1. Introduction

Desertification signifies land degradation in arid, semi-arid and dry sub-humid areas resulting from various factors including climatic variations and human activities (UNCCD, 2004). Desertification devastates land resources, diminishes ecosystem productivity, reduces ecological functions, and is deemed as a serious environmental problem in many arid, semi-arid, and dry sub-humid regions (Duan et al., 2014; Zhao et al., 2014). China is one of the countries that are susceptible to desertification. By 2014, predominantly in north and northwest China, the area of desertification covered 27.2% or 261, 1600 km^2, involving 18 provinces and 528 counties (State Forestry Administration, 2015). Desertification has caused direct economic loss of tens of billions RMB annually (Lu and Wu, 2002; Ge et al., 2016), and is also an essential obstacle to ecological safety and local socio-economic development, especially in northern China (Yang et al., 2005; Zhang et al., 2012; Qi et al., 2012; Wang et al., 2013).

Horqin Sandy Land, one of the four largest sandy lands, and belonging to an ecologically fragile region, agro-pastoral transitional, and semi-arid zone, is located in north China. Historically, the Horqin region was covered in grassland. However, population and food pressure has increased gradually since the 1950s (the “food for the program” policy was applied to settle pressure), leading to a major loss of grassland area (Song and Zhang, 2006). Anthropogenic activities were the primary causes of sandy desertification, including excessive reclamation, overgrazing, and extensive deforestation (Sui and Yuan, 2007; Wang et al., 2008; Lautenbach et al., 2011). Ground vegetation cover and topsoil loss have occurred through cultivation, livestock grazing and trampling (Pei et al., 2008; Verón et al., 2011; Kairis et al., 2013). Consequently, vegetation cover gradually decreased and soil was increasingly exposed to wind erosion, resulting in the sandy desertification area increasing from 42, 300 km^2 in 1959 to 61, 008 km^2 in 1987 (Wu, 2003).

To effectively manage sandy desertification, governments launched ecological restoration strategies, including the Three-North Shelterbelt Project (1978-present), the Grain for Green Project (1999–present), and the Beijing and Tianjin Sandstorm Source Treatment Project (2001–2010) (Li et al., 2017). Grazing exclusion was also employed by local governments, to prevent livestock from heavily grazing grassland (Miao et al., 2015). Previous studies confirmed that grazing exclusion

* Corresponding author.
E-mail address: xyan@cau.edu.cn (Y. Xu).

https://doi.org/10.1016/j.ecolind.2020.106215
Received 21 July 2019; Received in revised form 8 February 2020; Accepted 11 February 2020
Available online 26 February 2020

was effective in restoring natural vegetation, increasing soil nutrient availability, and improving biodiversity and ecosystem services (Li et al., 2012; Wu et al., 2014; Tang et al., 2016). The expansion of sandy desertification was gradually controlled in a governing context and the desertification area reduced to 32, 633 km^2 in 2015 from 52, 894 km^2 in 2000 (Duan et al., 2019). Vegetation was crucial for maintaining the ecological system security and services in ecologically fragile areas (Li et al., 2013). However, the Horqin Sandy Land is characterized by sand dunes alternating with interdune lowland (Liu et al., 2016) and environmental conditions, such as soil water content, nutrients, and particles, appear to be regulated by topography, which affects vegetation growth and distribution (Zuo et al., 2008). Thus, analyzing vegetation growth at different topographic positions is essential for rational land utilization, sustainable development, and optimized pattern.

There have been some studies on the relationship between topography and vegetation (Zhao et al., 2011; Gantsetseg et al., 2017). Svoray and Karnieli (2011) explored the temporal and spatial relationships between topography and aboveground net primary production of annuals in a semi-arid area. Wei et al. (2019) investigated the response of soil water content and aboveground biomass of grassland vegetation to precipitation and topography through field investigation. Zhou et al. (2019) analyzed vegetation growth at different topographic positions in Horqin zuoyihou Banner using derived land surface temperature (LST). Miyasaka et al. (2014) assessed the effects of different restoration measures and sand dune topography on vegetation restoration in the Horqin Sandy Land.

Vegetation index, derived from satellite images, has attracted more attention due to the advantage of time-saving and efficient. As a common vegetation index, NDVI can represent terrestrial vegetation growth (Zhang et al., 2013), because it is closely related to photosynthetically active radiation (Myneni et al., 1997). In previous studies, NDVI was widely used in crop area estimation (King et al., 2017; Song et al., 2017), crop mapping (Chen et al., 2018; Araujo Picoli et al., 2018), yield forecasting (Lai et al., 2018; Petersen, 2018), and vegetation monitoring (Li et al., 2017; Gao et al., 2017). Nevertheless, NDVI is susceptible to the soil background at low vegetation coverage and easy to saturate at high vegetation coverage (Huete et al., 1997; Nicholson and Farrar, 1994). This study, therefore, uses an improved vegetation index, GRNDVI (Zhao et al., 2011), to characterize the vegetation growth in Horqin area more accurately, and explores the changes in vegetation growth along topography and related factors.

Therefore, the main aims of this study were to: 1) analyze cropland and grassland growth at different topographic positions by calculating GRNDVI; 2) derive the soil wetness at different topographic positions; and 3) propose some methods to optimize the land use pattern based on vegetation growth and soil wetness to promote ecological balance and sustainable development.

2. Materials and methods

2.1. Study area

As one of the four largest sandy lands in China, Horqin Sandy Land is located in the east of Inner Mongolia and northeast of China. It lies between 117°49′ to 123°42′E and 41°41′ to 46°05′N, is composed of 15 counties and covers an area of 12.51×10^4 km^2 (Fig. 1). The study area is characterized by a typical semi-arid continental monsoon climate. The winter is cold and windy, summer is warm and rainy. The annual average temperature ranges from 3 to 7℃. The annual average precipitation ranges from 300 to 500 mm, and is mainly concentrated in summer, while the annual average evaporation varies between 1500 and 2500 mm. The altitude ranges from 24 to 2043 m, and decreases gradually from west to east. Aeolian sandy soil dominates this area, while other soil types include meadow, alkaline, and marsh. Three dune types alternate between fixed dune, semi-fixed dune, and shifting dune. Spring maize is the dominant crop in this area. Cropland and grassland are dominant land cover types in this area, accounting for 78.53% of the total area. The area of bareland is around half that of cropland, accounting for 14.47%. The area of other types, including wetland, water, forest, and impervious surface, is finite, accounting for merely 6.88% in total (Table 1).

2.2. Data set

Land cover data were collected from FROM-GLC10 (http://data.ess.tsinghua.edu.cn), which was based on 10-m Sentinel-2 data acquired in 2017 (Fig. 1). Several land cover types, including cropland, forest, grassland, shrubland, wetland, water, impervious surface and bare land were classified, and the overall accuracy was 72.76% (Gong et al., 2019). ASTER GDEM V002 was chosen to calculate a topography index, which is freely available at the spatial resolution of 30 m. Seven Landsat8 Operational Land Imager (OLI) images (L1T) from the 2017 summer were collected to calculate the vegetation index. These data were acquired from the US Geological Survey (USGS) Center for Earth Resources Observation and Science (EROS) (http://earthexplorer.usgs.gov/). The cloudiness of Landsat8 OLI images on the left part of the study area was high, which were inappropriate for this study. HJ-1 CCD images, therefore, with higher time resolution were selected. Additional 3 HJ-1 CCD images were downloaded from the China Center for Resource Satellite Data and Applications (CRESDA). HJ-1 satellite constellation comprises HJ-1A, HJ-1B, and HJ-1C. HJ-1A and HJ-1B are optical satellites and equipped with two CCD cameras. The temporal resolution can reach 2-days. The CCD data include four multispectral bands at 30 m spatial resolution (blue: 430–520 nm, green: 520–600 nm, red: 630–690 nm, near-infrared: 760–900 nm) (CCFRSDA, 2014). A total of ten images were chosen for this study, and are summarized in Table 2. A quadrat survey was conducted in Horqin zuoyihou Banner in July 2016 and July 2017. The topography is characterized by sand dunes alternating with undulating lowland areas in this Banner. Three dune types alternate between fixed dune, semi-fixed dune, and shifting dune. Sand plants, including herbaceous species and shrub species, were also distributed extensively. Five 1 × 1 m quadrats were selected randomly at five different slope positions to investigate the species, coverage, and height of herbaceous plants. For shrubs, three 5 × 5 m quadrats were correspondingly chosen. A handheld global positioning system (GPS) was used to record geographical locations and elevations of quadrats.

2.3. Methods

2.3.1. Image preprocessing

The preprocessing of images included radiometric calibration, atmospheric correction, mosaic, geometric registration, and GRNDVI calculation. Radiometric calibration was applied to convert the digital number (DN) to the TOA according to the Eq. (1):

$$L = DN / g + L_0 \quad (1)$$

where L represents the top of atmosphere radiance, DN is the digital number, and g and L_0 represent the gains and offsets, respectively.

Gains and offsets were provided in the metadata files of images. Spectral response functions for HJ-1 CCD sensors, downloaded from the China Center for Resource Satellite Data and Applications (CRESDA), were used to generate Spectral respond curves. The FLAASH (Fast Line-of-sight Atmospheric Analysis of Spectral Hypercube) module (Cooley et al., 2002) was employed to convert the top of atmosphere radiance into surface reflectance. Landsat images were mosaicked by the Seamless Mosaic tool in ENVI 5.3. For HJ-1 CCD images, automatic registration was utilized to reduce the error between adjacent images due to satellite scan time difference, with root mean square error (RMSE) controlled within 1 pixel. After automatic registration, three HJ-1 CCD images were mosaicked. Landsat 8-OLI (L1T) products have been orthorectified utilizing ground control points (GCP) and a digital elevation

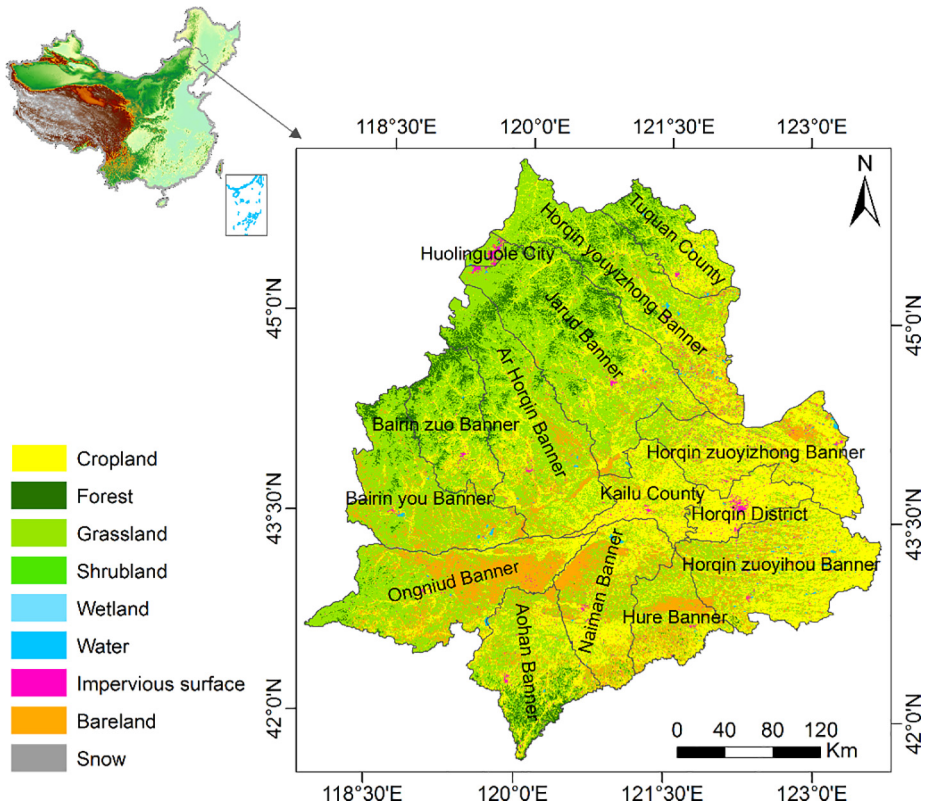

Fig. 1. Spatial distribution of land cover types in the study area.

Table 1
Area of land cover types in Horqin Sandy land.

Type	Area/ha	Percent/%
Cropland	3886432.15	31.08
Forest	684554.62	5.47
Grassland	5934154.93	47.45
Shrubland	15290.92	0.12
Wetland	3750.76	0.03
Water	43562.58	0.35
Impervious surface	129290.47	1.03
Bareland	1809006.35	14.47
Snow/Ice	0.06	0.00
Total	12506042.83	100

Table 2
Satellite data list.

Satellite	Path/row	Acquisition date
Landsat8-OLI	119/30	31 Aug.2017
Landsat8-OLI	120/29	21 Jul.2017
Landsat8-OLI	120/30	21 Jul.2017
Landsat8-OLI	121/28	29 Aug.2017
Landsat8-OLI	121/29	29 Aug.2017
Landsat8-OLI	121/30	28 Jul.2017
Landsat8-OLI	121/31	29 Aug.2017
HJ1A-CCD1	455/60	18 Jul.2017
HJ1A-CCD1	455/64	18 Jul.2017
HJ1A-CCD2	455/60	30 Jul.2017

model (DEM). Therefore, mosaicked Landsat 8 images were used as base images to warp the mosaicked HJ-1 CCD images, while the RMSE was less than 1 pixel. Considering the band differences of Landsat 8 and HJ-1 CCD images, we calculated corresponding GRNDVI separately firstly, a vegetation index, based on these 2 types of images. Then, the result of GRNDVI originating from different satellite images was

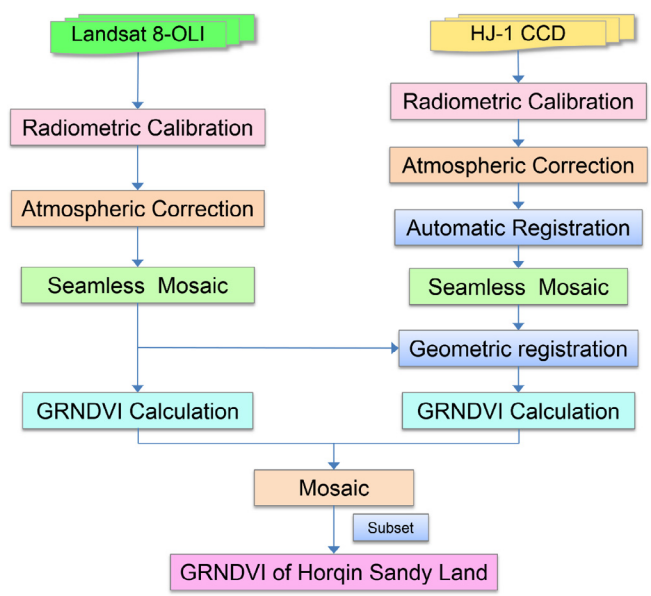

Fig. 2. Flow chart of image processing.

mosaicked. GRNDVI of Horqin Sandy Land was extracted by subset with vector boundary (Fig. 2).

2.3.2. Topography index (TI)

The focal statistics tool in ArcGIS was utilized to calculate the topography index based on the DEM, which was developed to reflect the relative topography in the study area. The mathematical expression of the topography index can be defined as:

$$TI = E - E_{mean} \quad (2)$$

where TI is the Topography index (m), E is the elevation of a pixel (m),

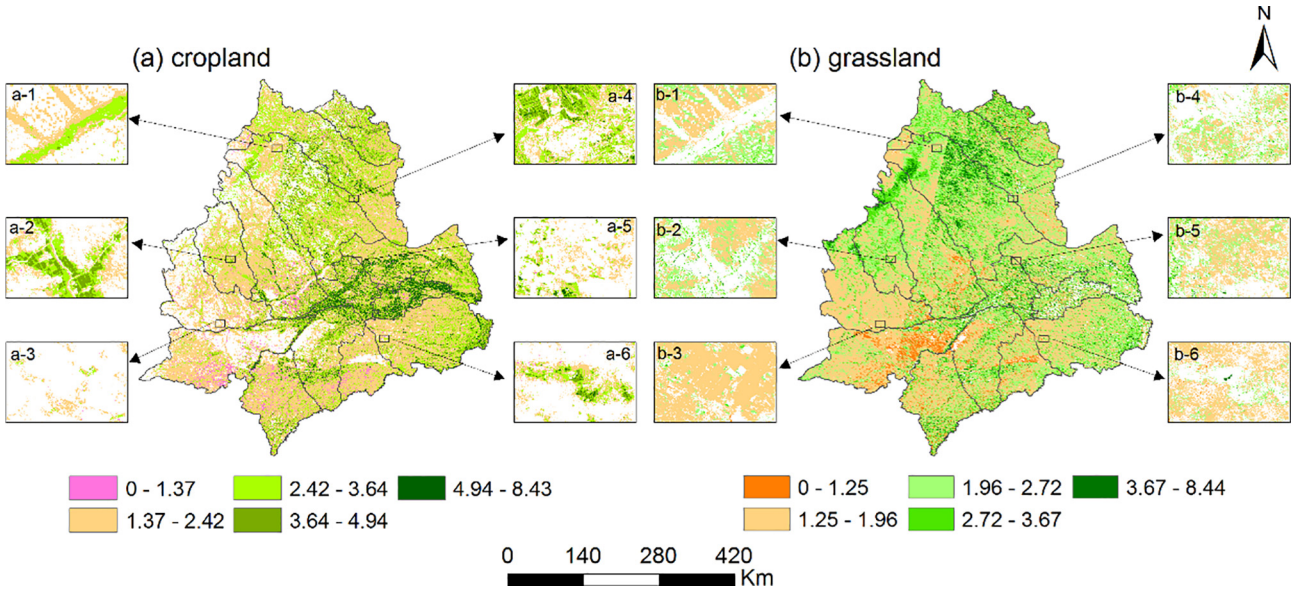

Fig. 3. GRNDVI distribution of cropland (a) and grassland (b) in the summer of 2017.

and E_{mean} is the average elevation of the pixels in the neighborhood (m). In the field surveys, the distances between topography positions (from the bottom of the slope to the top of the slope) of multiple dunes were observed to select an appropriate threshold. A rectangle with a width and height of 20 pixels (600 m × 600 m) was selected as the neighborhood type. When TI less than 0, it means the elevation of the pixel is lower than the surrounding pixels and vice versa.

2.3.3. GRNDVI

GRNDVI, the vegetation index used in this study, was developed and improved based on NDVI. The formula of NDVI can be transformed into Eq. (3), which indicates NDVI is related to ρ_{NIR}/ρ_R. In fact, ρ_{NIR}/ρ_R was simple ratio vegetation index (SR). Baret and Guyot (1991) analyzed the relationship between SR, NDVI, and LAI in detail. When the LAI is small, $\rho_R$is higher and ρ_{NIR} lower, and a small change in ρ_R has a greater effect on NDVI than SR. In contrast, under higher LAI, ρ_{NIR} is higher and ρ_R lower, and a small change in ρ_{NIR} produces a larger effect on SR than NDVI. To balance the change between SR and NDVI and increase their correlation with LAI, NDVI*SR was proposed by Gong et al. (2003) (Eq. (4)). The formula of NDVI*SR, however, enhanced vegetation index (VI) under high values and reduced VI under low values. The mathematical expression of the quadratic power could cause disproportionate changes in vegetation index. To improve this change, Zhao et al. (2011) squared the NDVI*SR and added 1 to NDVI to ensure results were positive. Thus, GRNDVI was generated and performed better than NDVI in both low and high vegetation cover. The formula was shown in Eq. (5).

$$\mathrm{NDVI} = \frac{\rho_{NIR} - \rho_R}{\rho_{NIR} + \rho_R} = \frac{\frac{\rho_{NIR}}{\rho_R} - 1}{\frac{\rho_{NIR}}{\rho_R} - 1} \tag{3}$$

$$\mathrm{NDVI} * \mathrm{SR} = \frac{\rho_{NIR} - \rho_R}{\rho_{NIR} + \rho_R} \times \frac{\rho_{NIR}}{\rho_R} \tag{4}$$

$$GRNDVI = \sqrt{\frac{\rho_{NIR}}{\rho_{RED}} \times \left(\frac{\rho_{NIR} - \rho_{RED}}{\rho_{NIR} + \rho_{RED}} + 1\right)} \tag{5}$$

where GRNDVI is the growth root normalized difference vegetation index; SR is simple ratio vegetation index; and ρ_{NIR} and ρ_{RED} are the reflectance in the electromagnetic spectrum at near-infrared band and red band, respectively.

2.3.4. Tasseled cap wetness

To understand plant growth patterns in spectral space, which belongs to the orthogonal transformation, the tasseled cap transformation (TCT) was proposed by Kauth and Thomas. (1976). Three components were generated from the TCT: Brightness, Greenness, and Wetness. The Brightness component is related to bare or partially covered soil, natural and man-made features, and varies in topography. The Greenness component measures the contrast between the visible bands and near-infrared band, which is the axis perpendicular to Brightness. The Wetness component is orthogonal to the Brightness and Greenness component and is relative to soil moisture, water, and other moisture features (Crist and Cicone, 1984; Crist and Kauth, 1986; Liu and Liu, 2009). Among the three components, Tasseled Cap Wetness has been used to assess changes in vegetation and soil (Skakun et al., 2003; Schultz et al., 2016; Mostafiz and Chang, 2018; Han et al., 2019). For the Landsat 8-OLI image, the Wetness component can be calculated as the following (Baig et al., 2014):

$$\begin{aligned}\text{Wetness} &= 0.1511 \times b2 + 0.1973 \times b3 + 0.3283 \times b4 + 0.3407 \times b5 - 0.7117 \\ &\quad \times b6 - 0.4559 \times b7\end{aligned} \tag{6}$$

where b2 to b7 are the corresponding bands of the Landsat 8 image.

3. Results

3.1. Spatial distribution of GRNDVI

Vegetation index measures can indicate the regional vegetation growth spatially. GRNDVI of cropland and grassland was calculated and Fig. 3a shows clearly the spatial distribution of GRNDVI of cropland in Horqin Sandy Land in the summer of 2017. GRNDVI in the east was higher than in the west, especially in the southeast, including Horqin district, Kailu County, Horqin Zuoyizhong Banner, east of Horqin zuoyihou Banner, and north of Naiman Banner. Cropland with higher GRNDVI values was also distributed in a strip rather than a sheet shape. Crop growth was relatively poor in the Hure, Aohan, Ongniudr, Bairin you, Bairin zuo, and west of Ar Horqin Banners where GRNDVI values were less than 2.42.

The spatial distribution of GRNDVI of grassland in the summer of 2017 is shown in Fig. 3b. Grassland growth in the north was better than other areas, especially in Jarud, Ar horqin, horqin youyizhong, and Bairin zuo Banners where the GRNDVI values were more than 2.72.

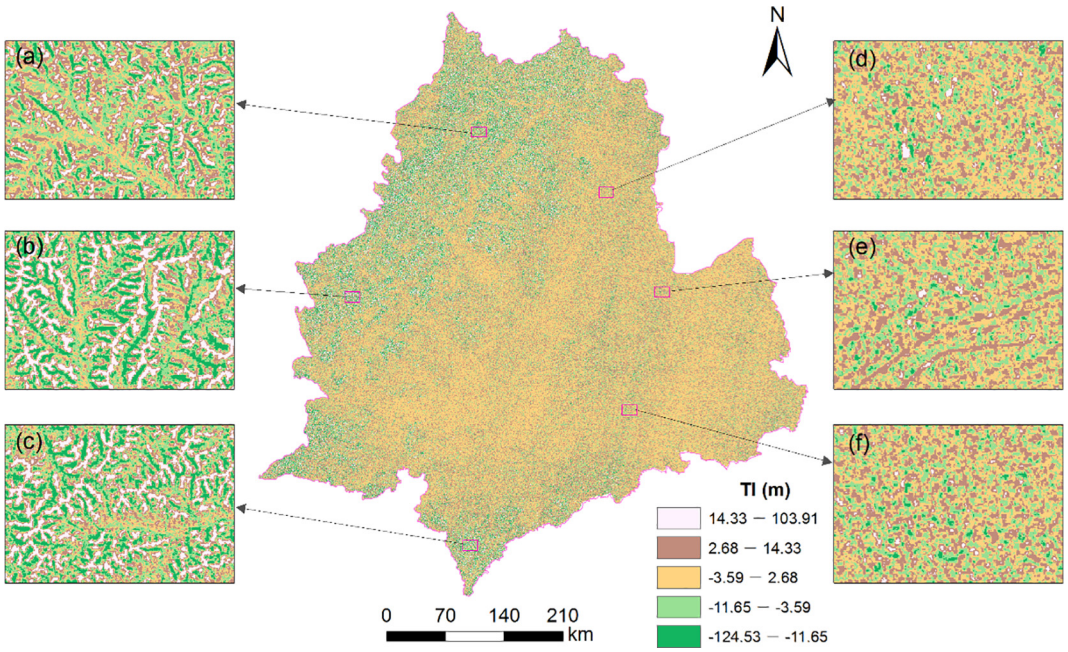

Fig. 4. Spatial distribution of topography index.

Meanwhile, GRNDVI values of the south were less than 1.96 mainly, including Aohan, Bairin you, Ongniud, and Hure Banners.

3.2. Topography index distribution

The spatial distribution of the Topography Index (TI) is shown in Fig. 4. Five groups were classified by using the natural breaks classification method, which aimed to reduce each class average deviation from the class mean and maximize every class deviation from the means of the other groups (Jenks, 1967; Aretano et al., 2015). TIs were mainly distributed at [−3.59, 2.68) m over 47% of the total area, followed by [2.68, 14.33) m over 24.37%, [−11.65, −3.59) m, and 20.65% respectively. TIs that less than −11.65 m and greater than 14.33 m were limited, accounting for 4.35% and 3.63% respectively.

TI spatial distribution was fragmented, values less than −11.65 m and greater than 14.33 m were concentrated in the northwest and southwest, while those in the range of [−11.65, −3.59), [−3.59, 2.68), and [2.68, 14.33) m were distributed extensively, especially in the central and eastern areas. Six TI samples were extracted to show more spatial detail. Samples, including a, b, and c (Fig. 4(a)-(c)), were extracted from the west and south of the study area, and contained 5 particular TI groups spatially distributed in strips. Meanwhile, samples including d, e, and f (Fig. 4(d)–(f)) extracted from the east of the study area, generally contained TIs in the range of [−11.65, −3.59), [−3.59, 2.68), and [2.68, 14.33) m, predominantly distributed in a patch shape.

3.3. GRNDVI changes with topography index

The overlay analysis tool in ArcGIS was employed to understand the relationship between GRNDVI and the Topography index. Fig. 5 illustrates cropland GRNDVI changes with increasing TI. Cropland GRNDVI increased a little initially and then decreased continuously. When TI was −124.53 to −11.65 m, GRNDVI of cropland was 2.97 but when TI increased to −11.65 to −3.59 m, corresponding GRNDVI increased to 2.98. GRNDVI of cropland decreased to 2.96, however, when TI was distributed at −3.59 to 2.68 m. Next, GRNDVI of cropland continued to decrease to 2.94 and 2.74 with TI increasing further. Therefore, cropland growth was highest when TI was distributed at −11.65 to −3.59 m and lowest at 14.33 to 103.91 m.

Fig. 6 illustrates grassland GRNDVI changes in different TIs.

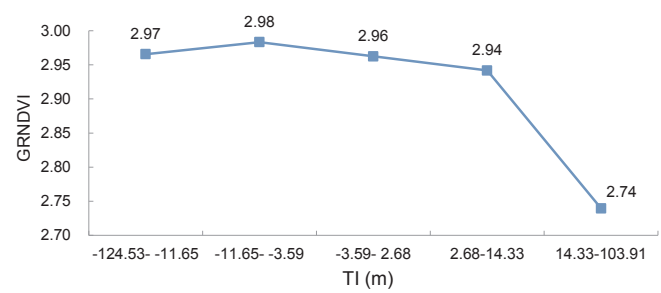

Fig. 5. Cropland GRNDVI changes in different TIs.

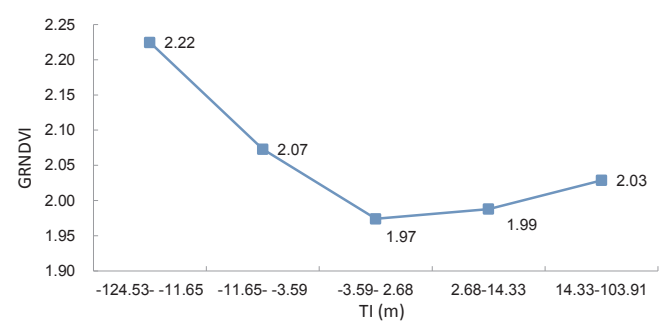

Fig. 6. Grassland GRNDVI changes in different TIs.

Grassland GRNDVI initially decreased and then increased. When TI was −124.53 to −11.65 m, GRNDVI of grassland was 2.22, but when TI was [−11.65, −3.59) and [−3.59, 2.68) m, corresponding GRNDVI were 2.07 and 1.97, respectively. However, grassland GRNDVI increased to 1.99, when TI was 2.68 to 14.33 m, and increased further to 2.03 when TI was 14.33 to 103.91 m. Therefore, grassland growth was highest when TI was distributed at −124.53 to −11.65 m and lowest at −3.59 to 2.68 m.

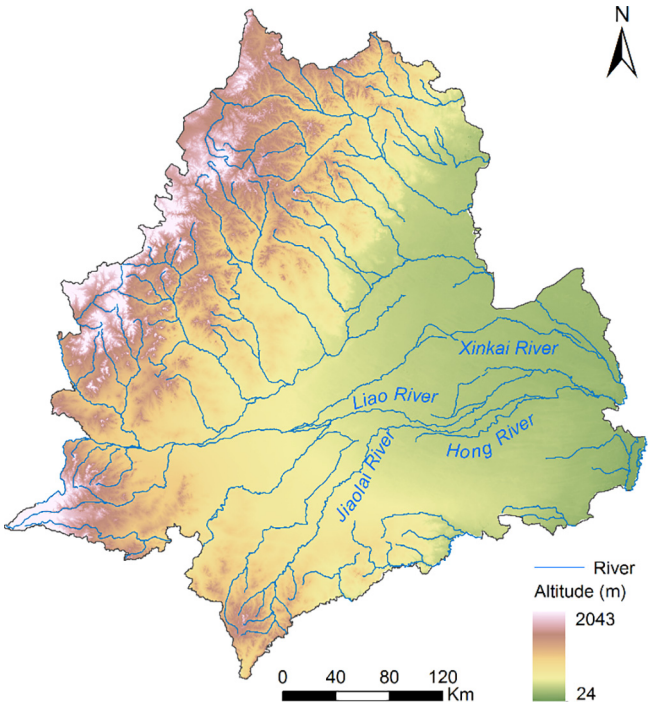

Fig. 7. Spatial distribution of DEM and rivers.

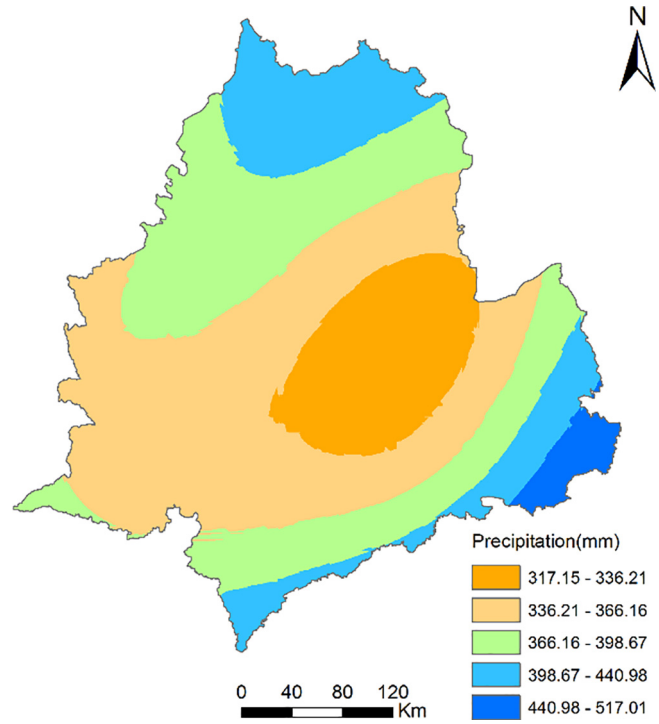

Fig. 8. Spatial distribution of precipitation.

4. Discussion

4.1. Spatial distribution of cropland and grassland GRNDVI

Horqin sandy land is a typical agro-pastoral transition zone, with a semi-arid climate typified by limited and highly variable annual precipitation. Water availability has a critical effect on cropland, which tends to have better growth when water is readily available. Fig. 7 shows the spatial distribution of DEM and rivers in Horqin Sandy Land, which reflects declining altitude from west to east. The topography of the east was lower and flatter than the west, which is more convenient for the development of agriculture, which is why the east has more cropland than the west. There are several rivers flowing from the west to east, including the Liao, Jiaolai, Xinkai, and Hong rivers, which provide convenient irrigation water for agriculture. Therefore, cropland adjacent to rivers has higher GRNDVI than away from rivers, and is the main reason for the distinct spatial distribution of cropland GRNDVI.

For grassland, precipitation and temperature may have more effect. Firstly, annual precipitation decreases gradually from the southeast to northwest owing to the monsoon. The topography of west, however, is mountains with high altitude. Thus, more precipitation is generated on windward slopes where water vapor is hindered by mountains. Therefore, annual precipitation initially decreases and then increases from southeast to northwest (Fig. 8). Precipitation in the north is higher than in the central area, and is also a basic source of supply for rivers in the north. Therefore, water resources are readily available for grassland in the north. Second, the altitude range of this area is 2019 m which reflects a temperature difference of about 12℃, since temperature decreases by 0.6℃ per 100 m rise in altitude. Therefore, temperature in the north is lower than in the south. Thus, the north is certainly more humid than the south and provides good natural conditions for grass growth, which may explain why the grasslands in the north have higher GRNDVI.

4.2. Cropland growth variation with topography index

Tasseled cap wetness was calculated to analyze soil moisture distribution in different TIs. HJ-1 CCD, on the left side of the study area, couldn't calculate the wetness with 4 bands. Landsat 8-OLI images, therefore, were employed to calculate wetness, which accounted for 71.82% of the total area after removing areas heavily affected by cloud (Fig. 9). Fig. 10 shows cropland mean wetness changes in different TIs. Cropland mean wetness initially increased slightly and then decreased continuously. When TI was −124.53 to −11.65 m, cropland mean wetness was −0.0163, but when TI increased to −11.65 to −3.59 m, it increased to −0.0136. Cropland mean wetness declined to −0.0142,

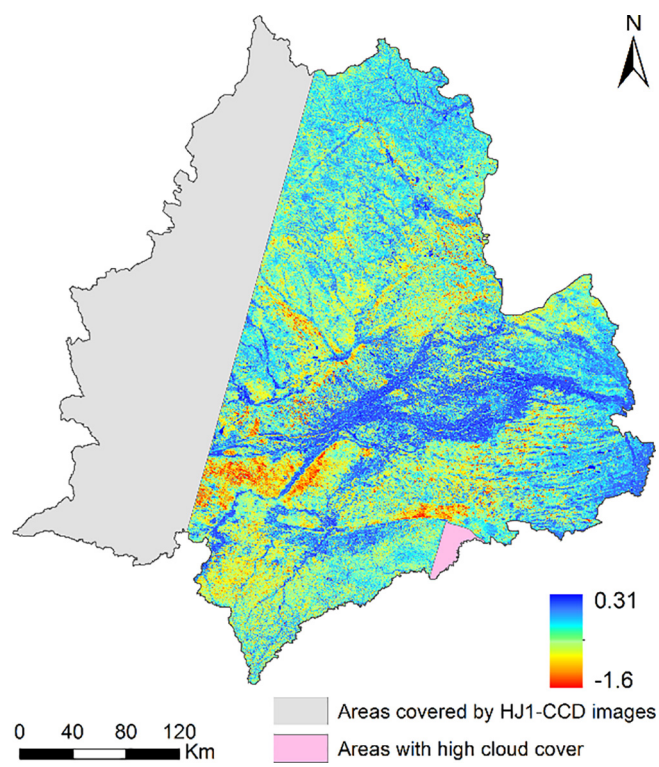

Fig. 9. Spatial distribution of wetness.

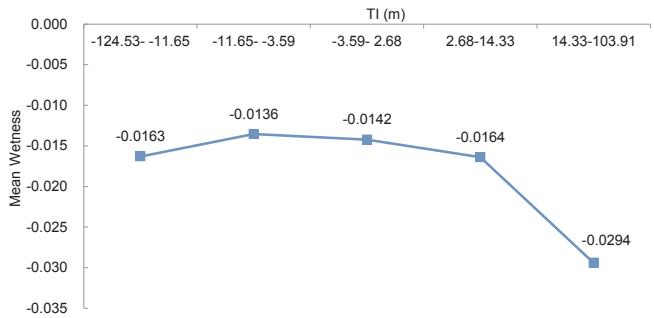

Fig. 10. Cropland mean wetness in different TIs.

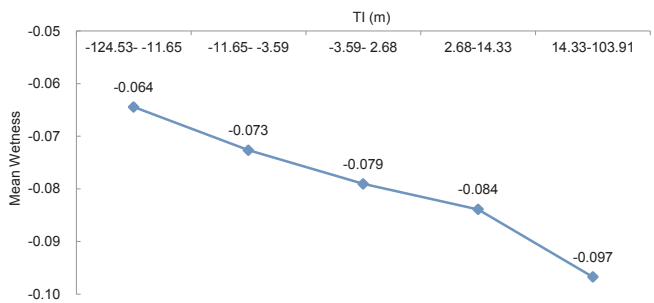

Fig. 11. Grassland mean wetness in different TIs.

however, when TI was −3.59 to 2.68 m. Finally, cropland mean wetness continued to decrease to −0.0164 and −0.0294 when TI increased further.

Tasseled cap wetness changes indicated variable soil moisture content along TIs to some extent. Soil moisture increased initially and then decreased with increasing TIs, indicating that it was affected by topography. Soil moisture was highest when TIs was between −11.65 and −3.59 m, followed by [−3.59, 2.68], [2.68, 14.33], and [−124.53, −11.65] m, while the lowest when TIs were 14.33 to 103.91 m. For the Horqin Sandy Land, the dominant sandy soil, with a coarse texture and loose structure, has a poor water-holding capacity. It is challenging to generate surface runoff when it rains due to rapid leakage. Soil tends to be wet in low-lying areas with a readily accessible

Table 3
Mean coverage and mean height of herb and shrub species at different slope positions.

Slope position	Herbaceous species		Shrub species	
	Coverage (%)	Height(cm)	Coverage (%)	Height(cm)
Hilltop	31.24	18.60	34.52	92.64
Upper slope	59.52	23.51	41.34	72.86
Mid slope	70.46	26.50	31.23	62.32
Lower slope	61.83	30.62	24.41	64.62
Flat	94.52	23.65	14.36	53.45

underground water table while drier in higher terrain with limit water supply. Soil water content decreases with increasing topography, which is consistent with Wei et al. (2019). Furthermore, water will be redistributed by changes in topography (Qiu et al., 2001; Schoorl et al., 2002). As a result, croplands on different topographies have distinctly different available water supplies, and therefore crop growth is different, resulting in differences in GRDNVI distribution. However, places where the terrain is too low can be waterlogged, and those that are too high may suffer water shortages and drought.

4.3. Grassland growth variation with topography index

Fig. 11 illustrates the grassland mean wetness changes in different TIs. Mean grassland wetness decreased continuously with increasing TI, which is distinct from the cropland mean wetness changes. When TI was −124.53 to −11.65 m, grassland mean wetness was −0.064, but when TI was between −11.65 and −3.59 m, it decreased to −0.073. Mean wetness of grassland was −0.079, −0.084 and −0.097 when TIs were [−3.59, 2.68], [2.68, 14.33], and [14.33, 103.91] m.

Grassland mean wetness changes indicate that grassland soil moisture decreased with increasing TIs. Changes in vegetation types, indicate this declining trend. According to the field survey, the main herbaceous species include *Juncus effuses, Eriochloa villosa, Thalictrum, Suaeda, miscanthus sacchariflorus*, and *Artemisia halodendron*. The Main shrub species include *Caragana microphylla, Lespedeza juncea,* and *Gueldenstaedtia stenophylla*. There are differences in the distribution of herbaceous and shrub species according to slope position (Fig. 12). Mean coverage of herbaceous species decreased gradually from flat to

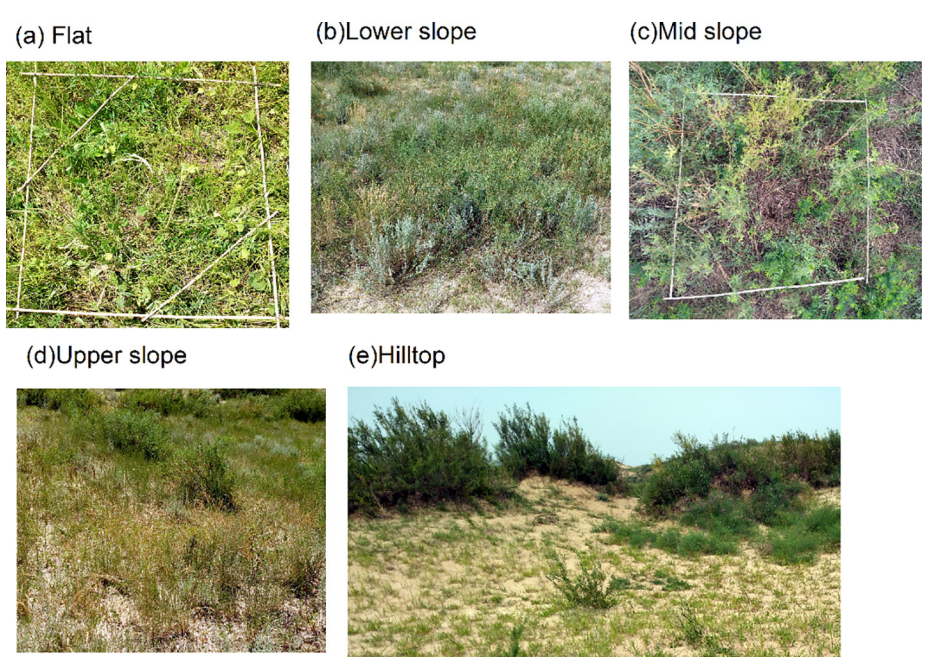

Fig. 12. Photographs of herb and shrub species at different slope positions.

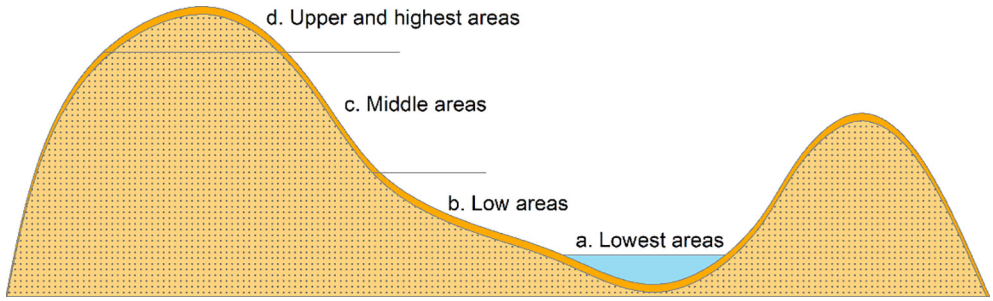

Fig. 13. Schematic diagram of topographic classes.

hilltop (Table 3), and mean height increased slightly at first and then declined. Mean coverage of shrub species was lower than herbaceous species overall, however, mean coverage and height of shrub species, increased slowly from flat to hilltop. This pattern indicates that herbaceous species are the dominant species while shrub species are subordinate. Herbaceous species are more common at low TIs, while shrub species tended to be more distributed at higher TIs. Soil water declined with increasing TIs, however, shrub species, including *Caragana microphylla*, are more drought tolerant than herbaceous plants due to their strong root systems that could access water even in deeper soil (Zhou et al., 2013; Xu et al., 1998) and therefore, could also survive in windy and sandy environments (Cao et al., 2008). Shrub growth was also indirectly affected by topographic position. Shrubs growing at higher topographic positions had higher photosynthetic activity, longer shoots, bigger leaves, and more biomass, with richer soil phosphorus availability and lower herbaceous aboveground biomass (Zhao et al., 2011). The development of shrubs could also improve soil physical and chemical properties significantly and facilitate the enrichment of herbaceous species with the "islands of fertility" (Yang et al., 2011; Zhao et al., 2007). GRNDVI of grassland declined initially and then increased, in agreement with Zhou et al. (2019). However, GRNDVI changes were also influenced by the distributional differences of plants whose positions were not only determined by soil water availability.

4.4. Land use suggestions

The terrain in Horqin Sandy Land is obviously highly variable. Therefore, it's important to optimize land utilization based on the natural condition at different topographic positions to promote sustainable development. The schematic diagram in Fig. 13 shows 4 topographic positions/classes. Class a is located in the lowest dunes, with optimal moisture conditions, and those also likely to have water accumulation. This situation is more suitable for a wetland rather than cropland, which could provide good habitat for some aquatic organisms and also protect biodiversity. Class b has relatively flat terrain and good moisture conditions, which is most appropriate for agricultural food production. Farmland infrastructures should be constructed and protected effectively here. Class c has inferior moisture conditions and terrain, which is not convenient for agricultural management but could be developed into grassland. Firstly, it would be suitable for growing the main herbaceous plants to improve the ecological environment, and secondly, it could be used to grow appropriate sandy pastures for local livestock. For class d, where soil moisture was poor and terrain is higher, crops would struggle, especially in the absence of ample precipitation. These sites should be planted with drought-tolerant shrub species and well protected to prevent land degradation.

5. Conclusion

This paper evaluated the effect of topography on cropland and grassland growth in Horqin Sandy Land. GRNDVI of vegetation and topography index were calculated, and spatial distribution of GRNDVI along a topography index was analyzed. GRNDVI was clearly influenced by topography, cropland growth initially increased and then decreased with increasing topography index, which was caused mainly by soil moisture difference on different terrains. Soil moisture initially increased and then decreased with a decreasing supply of underground water. Grassland growth decreased initially and then increased with increasing topography index and was caused by differences in soil moisture and plant species. Soil moisture decreased continuously with increasing topography index. Coverage and growth of herbaceous species were better in lower terrains while shrub species was better in high terrains. Different optimal land uses were proposed based on water availability and topographic conditions. In the lowest areas, wetlands could be developed to promote natural habitat for aquatic plants and animals. In low areas, water facilities could be constructed and crops planted to supply food. In the middle area, grassland should be utilized to provide some pastures. In the upper and highest areas, drought tolerant shrubs should be planted to stabilize slopes and enhance native biodiversity and ecological integrity. The findings of this paper could be used to optimize functional land utilization and promote sustainable development. We used wetness to represent the soil moisture distribution trend, but more field surveys may further refine the soil moisture gradient.

CRediT authorship contribution statement

Jiaqi Fan: Formal analysis, Software, Data curation, Writing - original draft, Writing - review & editing. **Yan Xu:** Conceptualization, Project administration, Funding acquisition, Writing - original draft, Writing - review & editing. **Haoyuan Ge:** Supervision, Validation, Visualization. **Wei Yang:** Investigation, Methodology, Resources.

Declaration of Competing Interest

The authors declare that they have no known competing financial interests or personal relationships that could have appeared to influence the work reported in this paper.

Acknowledgement

This research was supported by The National Natural Science Foundation of China [grant number 41301614].

References

Araujo Picoli, M.C., Camara, G., Sanches, I., Simoes, R., Carvalho, A., Maciel, A., Coutinho, A., Esquerdo, J., Antunes, J., Begotti, R.A., Arvor, D., Almeida, C., 2018. Big earth observation time series analysis for monitoring Brazilian agriculture. ISPRS J. Photogramm. Remote Sens. 145, 328–339. https://doi.org/10.1016/j.isprsjprs.2018.08.007.

Aretano, R., Semeraro, T., Petrosillo, I., De Marco, A., Pasimeni, M.R., Zurlini, G., 2015. Mapping ecological vulnerability to fire for effective conservation management of natural protected areas. Ecol. Modell. 295, 163–175. https://doi.org/10.1016/j.ecolmodel.2014.09.017.

Baig, M.H.A., Zhang, L., Shuai, T., Tong, Q., 2014. Derivation of a tasselled cap transformation based on Landsat 8 at-satellite reflectance. Remote Sens. Lett. 5, 423–431.

https://doi.org/10.1080/2150704X.2014.915434.
Baret, F., Guyot, G., 1991. Potentials and limits of vegetation indices for LAI and APAR assessment. Remote Sens. Environ. 35, 161–173. https://doi.org/10.1016/0034-4257(91)90009-U.
Cao, C., Jiang, D., Teng, X., Jiang, Y., Liang, W., Cui, Z., 2008. Soil chemical and microbiological properties along a chronosequence of Caragana microphylla Lam. plantations in the Horqin sandy land of Northeast China. App. Soil Ecol. 40, 78–85. https://doi.org/10.1016/j.apsoil.2008.03.008.
Chen, Y., Lu, D., Moran, E., Batistella, M., Dutra, L.V., Sanches, I.D., da Silva, R.F.B., Huang, J., Luiz, A.J.B., de Oliveira, M.A.F., 2018. Mapping croplands, cropping patterns, and crop types using MODIS time-series data. Int. J. Appl. Earth Obs. Geoinf. 69, 133–147. https://doi.org/10.1016/j.jag.2018.03.005.
Cooley, T., Anderson, G., Felde, G., Hoke, M., Ratkowski, A., Chetwynd, J., Gardner, J., Adler-Golden, S., Matthew, M., Berk, A., Bernstein, L., Acharya, P., Miller, D., Lewis, P., 2002. FLAASH, a MODTRAN4-based atmospheric correction algorithm, its application and validation. In: IGARSS 2002: IEEE International Geoscience and Remote Sensing Symposium and 24th Canadian Symposium on Remote Sensing, Vols I-Vi, Proceedings: Remote Sensing: Integrating Our View of the Planet, IEEE International Symposium on Geoscience and Remote Sensing (IGARSS). IEEE, pp. 1414–1418.
Crist, E.P., Cicone, R.C., 1984. A physically-based transformation of Thematic Mapper data—The TM Tasseled Cap. IEEE Trans. Geosci. Remote Sens. 22, 256–263. https://doi.org/10.1109/TGRS.1984.350619.
Crist, E.P., Kauth, R.J., 1986. The Tasseled Cap De-Mystified. Photogramm. Eng. Remote Sens. 52, 81–86.
Duan, H., Wang, T., Xue, X., Liu, S., Guo, J., 2014. Dynamics of aeolian desertification and its driving forces in the Horqin Sandy Land, Northern China. Environ. Monit. Assess. 186, 6083–6096. https://doi.org/10.1007/s10661-014-3841-3.
Duan, H., Wang, T., Xue, X., Yan, C., 2019. Dynamic monitoring of aeolian desertification based on multiple indicators in Horqin Sandy Land. China. Sci. Total Environ. 650, 2374–2388. https://doi.org/10.1016/j.scitotenv.2018.09.374.
Gantsetseg, B., Ishizuka, M., Kurosaki, Y., Mikami, M., 2017. Topographical and hydrological effects on meso-scale vegetation in desert steppe. Mongolia. J. Arid Land. 9, 132–142. https://doi.org/10.1007/s40333-016-0090-z.
Gao, F., Anderson, M.C., Zhang, X., Yang, Z., Alfieri, J.G., Kustas, W.P., Mueller, R., Johnson, D.M., Prueger, J.H., 2017. Toward mapping crop progress at field scales through fusion of Landsat and MODIS imagery. Remote Sens. Environ. 188, 9–25. https://doi.org/10.1016/j.rse.2016.11.004.
Ge, X., Dong, K., Luloff, A.E., Wang, L., Xiao, J., 2016. Impact of land use intensity on sandy desertification: an evidence from Horqin Sandy Land. China. Ecol. Indic. 61, 346–358. https://doi.org/10.1016/j.ecolind.2015.09.035.
Gong, Peng, Ruiliang, Pu., Biging, G.S., Larrieu, M.R., 2003. Estimation of forest leaf area index using vegetation indices derived from Hyperion hyperspectral data. IEEE Trans. Geosci. Remote Sens. 41, 1355–1362. https://doi.org/10.1109/TGRS.2003.812910.
Gong, P., Liu, H., Zhang, M., Li, C., Wang, J., Huang, H., Clinton, N., Ji, L., Li, Wenyu, Bai, Y., Chen, B., Xu, B., Zhu, Z., Yuan, C., Ping Suen, H., Guo, J., Xu, N., Li, Weijia, Zhao, Y., Yang, J., Yu, C., Wang, X., Fu, H., Yu, L., Dronova, I., Hui, F., Cheng, X., Shi, X., Xiao, F., Liu, Q., Song, L., 2019. Stable classification with limited sample: transferring a 30-m resolution sample set collected in 2015 to mapping 10-m resolution global land cover in 2017. Sci. Bull. 64, 370–373. https://doi.org/10.1016/j.scib.2019.03.002.
Han, L., Liu, D., Cheng, G., Zhang, G., Wang, L., 2019. Spatial distribution and genesis of salt on the saline playa at Qehan Lake, Inner Mongolia, China. Catena 177, 22–30. https://doi.org/10.1016/j.catena.2019.01.040.
Huete, A.R., Liu, H., van Leeuwen, W.J.D., 1997. Use of vegetation indices in forested regions: Issues of linearity and saturation, in: International Geoscience and Remote Sensing Symposium (IGARSS). Singapore, pp. 1966–1968. https://doi.org/10.1109/igarss.1997.609169.
Jenks, G.F., 1967. The data model concept in statistical mapping. Int. Yearbook Cartography 7, 186–190.
Kairis, O., Karavitis, C., Kounalaki, A., Salvati, L., Kosmas, C., 2013. The effect of land management practices on soil erosion and land desertification in an olive grove. Soil Use Manag. 29, 597–606. https://doi.org/10.1111/sum.12074.
Kauth, R.J., Thomas, G., 1976. The tasselled cap–a graphic description of the spectral-temporal development of agricultural crops as seen by Landsat, in: LARS Symposia. p. 159.
King, L., Adusei, B., Stehman, S.V., Potapov, P.V., Song, X.-P., Krylov, A., Di Bella, C., Loveland, T.R., Johnson, D.M., Hansen, M.C., 2017. A multi-resolution approach to national-scale cultivated area estimation of soybean. Remote Sens. Environ. 195, 13–29. https://doi.org/10.1016/j.rse.2017.03.047.
Lai, Y.R., Pringle, M.J., Kopittke, P.M., Menzies, N.W., Orton, T.G., Dang, Y.P., 2018. An empirical model for prediction of wheat yield, using time-integrated Landsat NDVI. Int. J. Appl. Earth Obs. Geoinf. 72, 99–108. https://doi.org/10.1016/j.jag.2018.07.013.
Lautenbach, S., Kugel, C., Lausch, A., Seppelt, R., 2011. Analysis of historic changes in regional ecosystem service provisioning using land use data. Ecol. Indic. 11, 676–687. https://doi.org/10.1016/j.ecolind.2010.09.007.
Li, J., Xu, B., Yang, X., Qin, Z., Zhao, L., Jin, Y., Zhao, F., Guo, J., 2017a. Historical grassland desertification changes in the Horqin Sandy Land, Northern China (1985–2013). Sci. Rep. 7. https://doi.org/10.1038/s41598-017-03267-x.
Li, X., Zhang, Z., Huang, L., Wang, X., 2013. Review of the ecohydrological processes and feedback mechanisms controlling sand-binding vegetation systems in sandy desert regions of China. Chin. Sci. Bull. 58, 1483–1496. https://doi.org/10.1007/s11434-012-5662-5.
Li, Y., Cao, Z., Long, H., Liu, Y., Li, W., 2017b. Dynamic analysis of ecological environment combined with land cover and NDVI changes and implications for sustainable urban–rural development: The case of Mu Us Sandy Land. China. J. Cleaner Prod. 142, 697–715. https://doi.org/10.1016/j.jclepro.2016.09.011.
Li, Y., Zhou, X., Brandle, J.R., Zhang, T., Chen, Y., Han, J., 2012. Temporal progress in improving carbon and nitrogen storage by grazing exclosure practice in a degraded land area of China's Horqin Sandy Grassland. Agric. Ecosyst. Environ. 159, 55–61. https://doi.org/10.1016/j.agee.2012.06.024.
Liu, Q., Liu, G., 2009. Using Tasseled Cap Transformation of CBERS-02 Images to Detect Dieback or Dead Robinia Pseudoacacia Plantation, in: 2009 2nd International Congress on Image and Signal Processing. Presented at the 2009 2nd International Congress on Image and Signal Processing (CISP), IEEE, Tianjin, China, pp. 1–5. https://doi.org/10.1109/CISP.2009.5304005.
Liu, X., He, Y., Zhao, X., Zhang, T., Li, Y., Yun, J., Wei, S., Yue, X., 2016. The response of soil water and deep percolation under Caragana microphylla to rainfall in the Horqin Sand Land, northern China. Catena 139, 82–91. https://doi.org/10.1016/j.catena.2015.12.006.
Lu, Q., Wu, B., 2002. Disaster assessment and economic loss budget of desertification in China. China Popul., Resour. Environ. 12, 29–33 (In Chinese with English Abstract).
Miao, R., Jiang, D., Musa, A., Zhou, Q., Guo, M., Wang, Y., 2015. Effectiveness of shrub planting and grazing exclusion on degraded sandy grassland restoration in Horqin sandy land in Inner Mongolia. Ecol. Eng. 74, 164–173. https://doi.org/10.1016/j.ecoleng.2014.10.004.
Miyasaka, T., Okuro, T., Miyamori, E., Zhao, X., Takeuchi, K., 2014. Effects of different restoration measures and sand dune topography on short- and long-term vegetation restoration in northeast China. J. Arid. Environ. 111, 1–6. https://doi.org/10.1016/j.jaridenv.2014.07.003.
Mostafiz, C., Chang, N.-B., 2018. Tasseled cap transformation for assessing hurricane landfall impact on a coastal watershed. Int. J. Appl. Earth Obs. Geoinf. 73, 736–745. https://doi.org/10.1016/j.jag.2018.08.015.
Myneni, R., Keeling, C., Tucker, C., Asrar, G., Nemani, R., 1997. Increased plant growth in the northern high latitudes from 1981 to 1991. Nature 386, 698–702. https://doi.org/10.1038/386698a0.
Nicholson, S.E., Farrar, T.J., 1994. The influence of soil type on the relationships between NDVI, rainfall, and soil moisture in semiarid Botswana. I. NDVI response to rainfall. Remote Sens. Environ. 50, 107–120. https://doi.org/10.1016/0034-4257(94)90038-8.
Pei, S., Fu, H., Wan, C., 2008. Changes in soil properties and vegetation following exclosure and grazing in degraded Alxa desert steppe of Inner Mongolia. China. Agric. Ecosyst. Environ. 124, 33–39. https://doi.org/10.1016/j.agee.2007.08.008.
Petersen, L.K., 2018. Real-Time Prediction of Crop Yields From MODIS Relative Vegetation Health: A Continent-Wide Analysis of Africa. Remote Sens. 10. https://doi.org/10.3390/rs10111726.
Qi, Y., Chang, Q., Jia, K., Liu, M., Liu, J., Chen, T., 2012. Temporal-spatial variability of desertification in an agro-pastoral transitional zone of northern Shaanxi Province, China. Catena 88, 37–45. https://doi.org/10.1016/j.catena.2011.08.003.
Qiu, Y., Fu, B., Wang, J., Chen, L., 2001. Spatial variability of soil moisture content and its relation to environmental indices in a semi-arid gully catchment of the Loess Plateau. China. J. Arid. Environ. 49, 723–750. https://doi.org/10.1006/jare.2001.0828.
Schoorl, J.M., Veldkamp, A., Bouma, J., 2002. Modeling Water and Soil Redistribution in a Dynamic Landscape Context. Soil Sci. Soc. Am. J. 66, 1610. https://doi.org/10.2136/sssaj2002.1610.
Schultz, M., Clevers, J.G.P.W., Carter, S., Verbesselt, J., Avitabile, V., Quang, H.V., Herold, M., 2016. Performance of vegetation indices from Landsat time series in deforestation monitoring. Int. J. Appl. Earth Obs. Geoinf. 52, 318–327. https://doi.org/10.1016/j.jag.2016.06.020.
Skakun, R.S., Wulder, M.A., Franklin, S.E., 2003. Sensitivity of the thematic mapper enhanced wetness difference index to detect mountain pine beetle red-attack damage. Remote Sens. Environ. 86, 433–443. https://doi.org/10.1016/S0034-4257(03)00112-3.
Song, N.P., Zhang, F.R., 2006. Re-evaluation on the food for the program policy and its impact on environment. Econ. Geogr. 26, 628–631 (In Chinese with English Abstract).
Song, X.-P., Potapov, P.V., Krylov, A., King, L., Di Bella, C.M., Hudson, A., Khan, A., Adusei, B., Stehman, S.V., Hansen, M.C., 2017. National-scale soybean mapping and area estimation in the United States using medium resolution satellite imagery and field survey. Remote Sens. Environ. 190, 383–395. https://doi.org/10.1016/j.rse.2017.01.008.
State Forestry Administration, 2015. A Bulletin of Status Quo of Desertification and Sandification in China [WWW Document]. A Bulletin of Status Quo of Desertification and Sandification in China. URL http://www.forestry.gov.cn/main/65/20151229/835177.html (accessed 6.3.19).
Sui, Y., Yuan, H., 2007. Agroecological and economic approach of prevention and curing of sandstorms in China. Ecol. Econ. 61, 129–133. https://doi.org/10.1016/j.ecolecon.2006.02.008.
Svoray, T., Karnieli, A., 2011. Rainfall, topography and primary production relationships in a semiarid ecosystem. Ecohydrology 4, 56–66. https://doi.org/10.1002/eco.123.
Tang, J., Davy, A.J., Jiang, D., Musa, A., Wu, D., Wang, Y., Miao, C., 2016. Effects of excluding grazing on the vegetation and soils of degraded sparse-elm grassland in the Horqin Sandy Land. China. Agric. Ecosyst. Environ. 235, 340–348. https://doi.org/10.1016/j.agee.2016.11.005.
UNCCD, 2004. Preserving our common ground. In: UNCCD 10 Years on United Nations Convention to Combat Desertification. Bonn, Germany.
Verón, S.R., Paruelo, J.M., Oesterheld, M., 2011. Grazing-induced losses of biodiversity affect the transpiration of an arid ecosystem. Oecologia 165, 501–510. https://doi.org/10.1007/s00442-010-1780-4.
Wang, F., Pan, X., Wang, D., Shen, C., Lu, Q., 2013. Combating desertification in China: past, present and future. Land Use Policy 31, 311–313. https://doi.org/10.1016/j.landusepol.2012.07.010.

Wang, X., Chen, F., Hasi, E., Li, J., 2008. Desertification in China: an assessment. Earth Sci. Rev. 88, 188–206. https://doi.org/10.1016/j.earscirev.2008.02.001.

Wei, P., Pan, X., Xu, L., Hu, Q., Zhang, X., Guo, Y., Shao, C., Wang, C., Li, Q., Yin, Z., 2019. The effects of topography on aboveground biomass and soil moisture at local scale in dryland grassland ecosystem. China. Ecol. Indic. 105, 107–115. https://doi.org/10.1016/j.ecolind.2019.05.002.

Wu, W., 2003. Dynamic Monitor to Evolvement of Sandy Desertified Land in Horqin Region for the Last 5 Decades, China. J. Desert Res. 23, 646–651 (In Chinese with English Abstract).

Wu, X., Li, Z., Fu, B., Zhou, W., Liu, H., Liu, G., 2014. Restoration of ecosystem carbon and nitrogen storage and microbial biomass after grazing exclusion in semi-arid grasslands of Inner Mongolia. Ecol. Eng. 73, 395–403. https://doi.org/10.1016/j.ecoleng.2014.09.077.

Xu, X., Zhang, R., Xue, X., Zhao, M., 1998. Determination of evapotranspiration in the desert area using lysimeters. Commun. Soil Sci. Plant Anal. 29, 1–13. https://doi.org/10.1080/00103629809369924.

Yang, X., Zhang, K., Jia, B., Ci, L., 2005. Desertification assessment in China: an overview. J. Arid. Environ. 63, 517–531. https://doi.org/10.1016/j.jaridenv.2005.03.032.

Yang, Z.P., Zhang, Q., Wang, Y.L., Zhang, J.J., Chen, M.C., 2011. Spatial and temporal variability of soil properties under Caragana microphylla shrubs in the northwestern Shanxi Loess Plateau. China. J. Arid. Environ. 75, 538–544. https://doi.org/10.1016/j.jaridenv.2011.01.007.

Zhang, G., Dong, J., Xiao, X., Hu, Z., Sheldon, S., 2012. Effectiveness of ecological restoration projects in Horqin Sandy Land, China based on SPOT-VGT NDVI data. Ecol. Eng. 38, 20–29. https://doi.org/10.1016/j.ecoleng.2011.09.005.

Zhang, G., Zhang, Y., Dong, J., Xiao, X., 2013. Green-up dates in the Tibetan Plateau have continuously advanced from 1982 to 2011. Proc. Natl. Acad. Sci. U.S.A. 110, 4309. https://doi.org/10.1073/pnas.1210423110.

Zhao, H., Yang, Z., Li, L., Di, L., 2011. Improvement and comparative analysis of indices of crop growth condition monitoring by remote sensing. Transactions of the CSAE 27, 243–249. https://doi.org/1002-6819 (2011)-01-0243-07(In Chinese with English Abstract).

Zhao, H.-L., Li, J., Liu, R.-T., Zhou, R.-L., Qu, H., Pan, C.-C., 2014. Effects of desertification on temporal and spatial distribution of soil macro-arthropods in Horqin sandy grassland, Inner Mongolia. Geoderma 223–225, 62–67. https://doi.org/10.1016/j.geoderma.2014.01.026.

Zhao, H.-L., Zhou, R.-L., Su, Y.-Z., Zhang, H., Zhao, L.-Y., Drake, S., 2007. Shrub facilitation of desert land restoration in the Horqin Sand Land of Inner Mongolia. Ecol. Eng. 31, 1–8. https://doi.org/10.1016/j.ecoleng.2007.04.010.

Zhao, T., Li, J., Zhang, X., Zhao, N., Gao, Y., 2011b. Photosynthetic and morphological characters of Caragana microphylla in different slope aspects and positions. Acta Ecol. Sin. 31, 163–168. https://doi.org/10.1016/j.chnaes.2011.03.007.

Zhou, J., Xu, Y., Gao, Y., Xie, Z., 2019. Land use model research in agro-pastoral ecotone in northern China: a case study of Horqin Left Back Banner. J. Environ. Manage. 237, 139–146. https://doi.org/10.1016/j.jenvman.2019.02.046.

Zhou, Y., Chen, J., Chen, X., Cao, X., Zhu, X., 2013. Two important indicators with potential to identify Caragana microphylla in xilin gol grassland from temporal MODIS data. Ecol. Indic. 34, 520–527. https://doi.org/10.1016/j.ecolind.2013.06.014.

Zuo, X., Zhao, H., Zhao, X., Guo, Y., Li, Y., Luo, Y., 2008. Plant distribution at the mobile dune scale and its relevance to soil properties and topographic features. Environ. Geol. 54, 1111–1120. https://doi.org/10.1007/s00254-007-1104-0.